GroundWinds New Hampshire and the LIDARFest 2000 Campaign

Carl A. Nardell, Paul B. Hays, Jane Pavlich, Michael Dehring, Greg Sypitkowski
Michigan Aerospace Corporation, Ann Arbor, MI

ABSTRACT

The GroundWinds New Hampshire instrument is a direct detection Doppler LIDAR system that utilizes backscatter signal from both Rayleigh and Mie scattering to measure Doppler shifts in the atmosphere from the ground. This system is the first of two planned systems that will be used to validate the technology and improve the design for other potential implementations. As a means to that end, a validation campaign was conducted in September 2000 to compare the GroundWinds measurements to that from four other systems. These were the GLOW instrument, the NOAA Mini MOPA system, and a Microwave sounder from the National Weather Service. This paper will review the design of the GroundWinds instrument, as well as summarize some of the preliminary GroundWinds results from the field experiment.

Key words: direct detection, LIDAR, GroundWinds, Doppler, Fabry-Perot

1. INTRODUCTION

The incoherent lidar system investigated here makes use of a Fabry-Pérot interferometer as a high spectral resolution element, capable of detecting Doppler shifts of the backscattered signal that correspond to velocities less than 1 ms^{-1}. A schematic of a conceptual system configuration is presented in Fig. 1. In this figure, the spectrum of the return signal is shown. This spectrum is recorded as a function of time to deduce Doppler shift of the light as a function of altitude. It should be noted that this spectrum consists of two distinct components. These are a broad return that is caused by Rayleigh scattering from atmospheric gases, and a narrow return that is the result of Mie scattering from atmospheric aerosols. The GroundWinds system utilizes both of these components to produce a measurement of wind velocity. The aerosol component, when present allows for very accurate wind measurement (less than 1 m/s), but cannot always be relied upon, as aerosol concentrations vary greatly. The molecular component is always present, and is the primary source used for wind measurement. Each of these components is measured using an interferometer whose resolution is optimized for that measurement. The instrument is optimized for the Raleigh (molecular) return, but it is configured to fully utilize the Mie scatter (aerosol) return, when available.

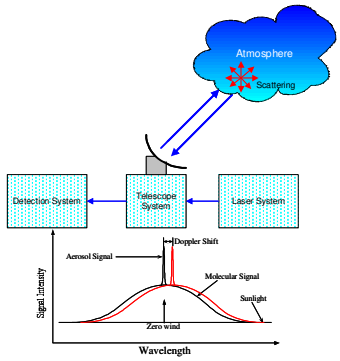

Figure 1: Direct detection Doppler LIDAR. This figure illustrates how transmitted laser light, which has been scattered by the atmosphere, is gathered by a telescope and processed by the detection system. The GroundWinds detection scheme is a simple high-resolution incoherent interferometer based on the flight qualified High Resolution Doppler Imager (HRDI) optical system that is currently operating on the Upper Atmosphere Research Satellite (UARS). HRDI provides winds by passive measurement of absorption and emission lines in the Earth's stratosphere, mesosphere, and lower thermosphere (Hays et al., 1993).

What follows is a description of the GroundWinds direct detection LIDAR system. We note that this system is functionally identical to a space LIDAR, but most subsystems are composed of commercial parts to minimize cost and simplify maintenance and serviceability. This is an issue since this system will be actively used on a daily basis as a research tool.

The key elements of GroundWinds are: a) the interferometer, b) the laser, c) the transmitting telescope, d) the receiving telescope, and e) an instrument control and data processing system. The following discussion describes the instrument beginning with the outgoing laser beam and progressing through to the detectors. This system is also illustrated in a more schematic form in Figure 2 where the functional relationships between the optical components are shown in a more physical layout.

The laser beam exits the instrument through a beam expander, which reduces the divergence angle of the emerging light. This narrow transmitted beam allows the receiving telescope to use a small field of view to minimize the system etendue, reduce the size of detection optical system, and also results in minimum stray light being transmitted to the detectors. The laser light beam is scattered by the molecules and aerosols in the atmosphere resulting in a detectable backscattered light signal. This back-scattered light is collected by the primary receiving telescope which tracks the laser beam as the laser beam expander and telescope are rotated in azimuth to observe horizontal components of the wind. A fiber optic cable carries the scattered light from the main receiving telescope to the interferometer subsystem. An active alignment system is utilized to track the laser beam as the telescope bearing wobbles with azimuth rotation. The outgoing signal light is introduced into the primary optical chain through a mirror

system, which allows a very small leakage of light from the primary laser beam to be used as a wavelength reference for the detectors. The primary signal light and the reference beam are then passed through a narrow-band filter system composed of a dielectric filter and a low resolution Fabry-Pérot etalon. After filtering, the light is introduced into the molecular interferometer and the resulting spectrum is focused into the patented Circle to Line Interferometer Optical system (CLIO). This innovative device converts the circular fringes from the Fabry-Pérot into a linear pattern that is detected with a charge-coupled device (CCD). The circular fringe pattern that is created by the molecular etalon is present in the transmitted light, the reflected light from the etalon being the complement of the transmitted fringe pattern. In most interferometers, the reflected light is lost from the system and represents a significant inefficiency. However, in the GroundWinds interferometer the reflected light from the molecular etalon is transmitted into the aerosol etalon via a fiber optic. Here again the etalon creates a velocity sensitive circular fringe pattern that is transformed into a linear pattern by a CLIO coupled to a CCD camera. The reflected light is used to illuminate a photomultiplier tube (PMT). The PMT is used to measure a photometric intensity profile. This can be used to measure integrated energy returned, and has value in numerically correcting for any misalignment in the etalons. The system detectors record at any one time three sets of information; 1) the aerosol fringe pattern optimized to detect the motion of aerosols, 2) the molecular direct fringe pattern, optimized to detect the motion of the molecular component of the atmosphere, and 3) the integrated photometric return.

Unlike other LIDARs, this system utilizes a unique CCD imaging technology to determine simultaneously the range and spectrum of the backscattered light. There are several advantages of using CCD's as the primary detectors. First, the CCDs used in GroundWinds provide approximately a 10:1 improvement in detector sensitivity over older technologies such as photo-multiplier tubes (PMT) and the image plane detectors used in the HRDI instrument. Secondly, the use of a CCD allows electronically programmable range resolution and spectral resolution. These are very useful properties for this instrument.

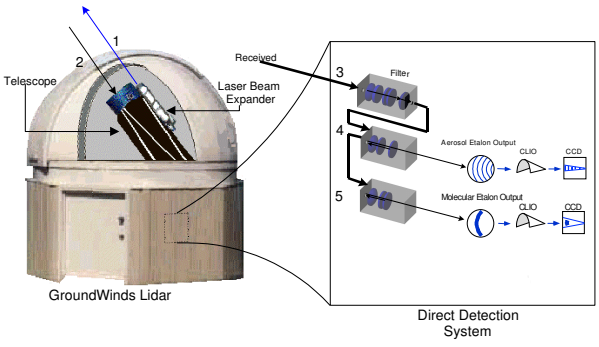

Figure 2: A depiction of the entire optical system is shown here schematically. This graphic depicts how the returned light from the atmosphere is collected by the telescope, coarsely filtered by an interference filter and low resolution Fabry-Pérot etalon, and finally how the detailed spectrum is filtered by the high resolution etalon. The output of this detector channel is recorded in a unique fashion on a CCD detector.

2. INSTRUMENT OVERVIEW

Interferometer

In order to explain how this system works, it is necessary to describe a significant feature of the Fabry-Pérot. The Fabry-Pérot is often touted as an efficient user of light, and in some respects this is true (Jacquinot, 1954). However, the device actually discards a significant portion of the incident light. If one order of a Fabry-Pérot with plate reflectivity R is projected onto a detector, a fraction $[(1-R)/(1+R)]$ of the light incident on the etalon is actually transmitted while the rest is reflected. This reflected light amounts to a fraction $2R/(1+R)$. For example, if R=0.90 then 95% of the light is reflected. If less than a full free spectral range is projected on the detector, then a somewhat higher fraction of the light is transmitted. This is the reason that some studies of incoherent lidar have projected less than a full free spectral range on the detector (Hays et al., 1984; Rees and McDermid, 1990), in an effort to keep the size of the instrument to a minimum. Figure 3 shows the optical configuration in which GroundWinds utilizes the Fabry-Perot. Note that the input fiber is not located on the optical axis.

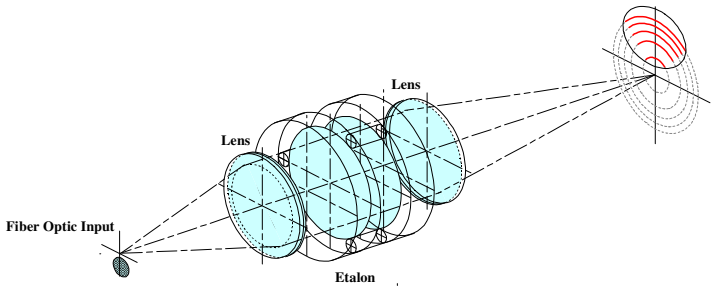

Figure 3: Fabry-Perot optical configuration

Figure 4(a) shows the transmission curves for an etalon with a gap of 15 cm and a plate reflectivity of 0.90. We have demonstrated that this is near optimal for measuring the aerosol backscatter. The maximum transmittance is about 50%, which is less than unity as the result of the losses and defects assumed for this etalon. The reflectivity of the entire etalon is simply one minus the etalon transmission, which is valid because the absorption losses in etalons with dielectric coatings are very small and any scattering losses are very narrow angle and do not diverge much from the specular beam. This reflected light is then used as the input for a second etalon that is optimized for molecular scattering (it has a much smaller gap, ~1.8 cm and comparable plate reflectivity.). We recognize that the light reflected by the molecular etalon still contains spectral information.

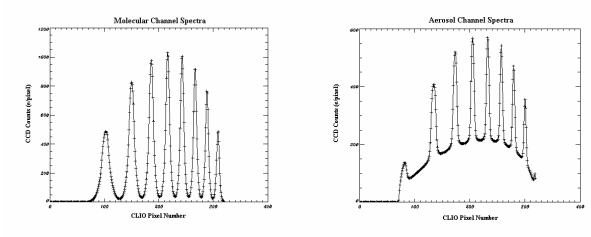

Fig. 4 (a) Response function of the molecular system. Eight orders have been projected onto the detector. The shape is characterized by the instrument function convolved with the return spectral shape. (b) Response function of the aerosol system. Here again eight orders have been projected onto the detector

Thus, the GroundWinds detection system uses two etalons: 1) a very high-resolution etalon optimized for the aerosol return; and 2) a lower-resolution channel optimized for the molecular return. This system is shown in block diagram form in figure 5. In depth descriptions of system components are provided in subsequent sections.

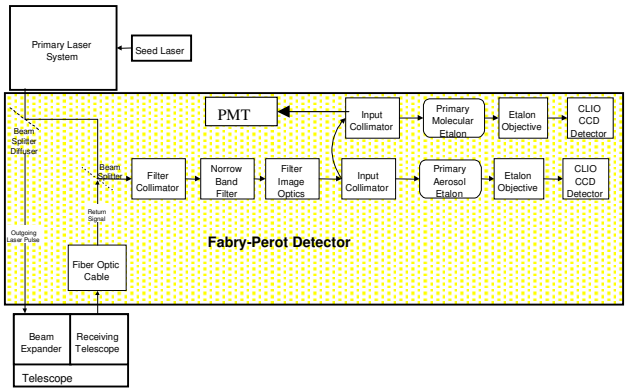

Figure 5: The detection system employs three detectors for the following three components: 1) the light transmitted by the aerosol system, 2) the light reflected by the aerosol channel and transmitted by the molecular etalon, and 3) the light reflected by the aerosol channel and reflected by the molecular etalon. This system collects every photon and is therefore much more efficient than any other previously considered or proposed incoherent system. Most photons are used in the molecular channel, reducing the maximum wind error as much as possible. The optimization of the system is described in section 4.3 and the optics necessary for the system have been designed and are described in section 6.4.

Table 1: Interference Filters.

Central wavelength	532 nm
Type	Multicavity, dielectric
Broad Band Filter FWHH	3.0 nm
Peak Transmittance	0.65

Table 2: Filter Etalon

Gap	0.1 cm
Reflectivity Effective coated diameter	0.9 2.8 cm
Plate diameter	6.0 cm
Coated aperture	3.0 cm.
Focal Length of Collimator	6.0 cm. (GPX-25-60-2)
Focal Length of Objective	6.0 cm. (GPX-25-60-2)
Finesse	20
Spacing type	PZT tunable

Table 3: Aerosol Etalon

Plate spacing	15 cm
Index of refraction	1.00
Number of orders	6.5
Free spectral range	0.03333 cm^{-1}
Plate diameter	6.0 cm
Coated aperture	4.4 cm
Working aperture	4.4 cm.
Dynamic range	266 ms^{-1}/order
Reflectivity	0.86
Etalon defects (1/e)	5 nm
Loss per plate	0.01
Number of channels	312
Focal Length of Collimator	10.0 cm. (GPX-50-150-5)
Focal length of Objective	70.0 cm (CPX10506 JML)
f/number	2.3
Spacing type	PZT tunable

Table 4: Molecular Etalon

Plate spacing	1.85 cm gap.
Number of orders	7.8
Free spectral range	0.3333 cm^{-1}
Plate diameter	6.0 cm
Coated aperture	4.0 cm
Working aperture	2.6 cm.
Dynamic range	2660 ms^{-1} /order
Reflectivity	0.86
Etalon defects (1/e)	5 nm
Loss per plate	0.01
Number of channels	312
Focal Length of Collimator	6.0 cm (GPX-25-60-2)
Focal length of objective	26.0 cm (DBL14182 JML)
f/number	2.3
Spacing type	PZT tunable

CLIO

The Fabry-Pérot interference pattern for a conventional interferometer appears as a set of concentric rings at the infinity focus of the interferometer objective lens, where the

detector system is located. The left portion of figure 7 shows this interference pattern as it would appear in the image plane of a conventional instrument. A technique for converting the circular fringes of a Fabry-Pérot interferometer into a linear pattern which can be detected with a conventional linear detector has been described by Hays (1990). The technique, called the Circle to Line Interferometer Optical system (CLIO, U.S. Patent #4,893,003), simplifies the analysis of interferometric information by converting the circular rings, or fringes, into a linear pattern similar to that produced by a conventional spectrometer.

The specific optical technique used to produce this linear interference pattern is to transform the rings that appear at the infinite focus of the objective lens in a Fabry-Pérot interferometer into a series of line segments on the axis of a 45° half-angle internally reflecting cone. In practice the transformation may be accomplished using a 90° sector of a cone to transform a 90° sector of the circular ring pattern on to the cone axis. The GroundWinds interferometers operate with a 90° sector of the fringe plane, which is illuminated by a fiber optic array. The basic optical configuration is illustrated schematically in Fig. 8. Here the cone is shown to be situated with its vertex on the optical axis in the focal plane of the main objective lens of the Fabry-Pérot optical system, where the ray bundles are focused. The cone acts as a very astigmatic element that focuses all meridional rays of light which would intersect a circle in the fringe plane at a point on the cone axis. Rays which are not in the meridional plane tend to be focused on a line that is perpendicular to the cone axis at the same axial distance from the vertex. In principle, this transformation results in no degredation of the optical signal. In practice, the surface quality of the CLIO optic must be very high so that scatter and absorption are not a problem.

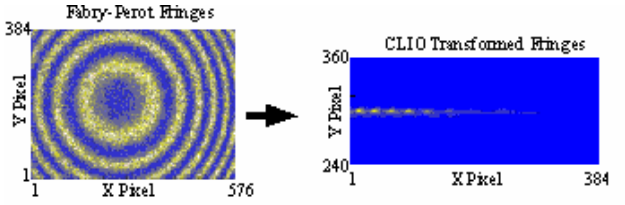

Figure 7: Transformation of Fabry-Perot fringes performed by CLIO

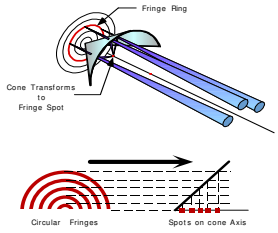

Figure 8: Conceptual ray trace showing the CLIO concept

Light Recycling

The GroundWinds instrument measures both molecular and aerosol backscatter with two separate and independent detectors. The light from each laser pulse in the GroundWinds instrument is used to serve both channels. This was only possible through the development of a light recycler that utilizes the reflected light from the etalon plates of the molecular channel to feed the aerosol channel. This innovation was very important because it allows the simultaneous determination of Doppler shifts from Mie scattering as well as Rayleigh. We refer to this as light recycling (U.S. patent #6,163,380), and can be used not only as a way of injecting the signal into two interferometers, but also as a means of reintroducing the signal into a channel multiple times to improve the throughput of a single channel.

The implementation of this idea is accomplished through the use of fiber optic arrays. These arrays use a single multimode fiber optic to introduce the light into the interferometer off-axis. The rejected light appears at the other side of the optical axis at an equal distance. If a fiber optic is positioned at the point where this rejected light is in focus, it can be collected and reintroduced at a point on the same side of the axis where it was initially injected. This can be done many times in an effort to force as much light as possible through the instrument. It should be noted that the fiber optic has the unique and important property of eliminating spatial coherence while maintaining spectral coherence. This is the essence of the direct detection technique. It might be hypothesized that a mirror could be used for this recycling technique, but in fact, a mirror would not be effective, as the spatial coherence must be destroyed in order to yield significant throughput on subsequent recycling.

It should be noted that the increase in throughput results from the increased divergence through the instrument that this additional illumination offers without a need to increase the clear aperture of the instrument. As the number of recycles increases, the width of the instrument function on the detector does grow. This necessitates an increase in detector speed to preserve spatial resolution.

The fiber optic ferule that is used to accomplish this task is shown in figure 9. This fiber optic array is placed at the input plane at the focal plane of the collimating lens. In this implementation, the light is recycled twice through the instrument.

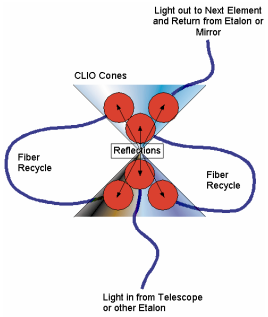

Figure 9: Schematic of the fiber optic ferule used for light recycling.

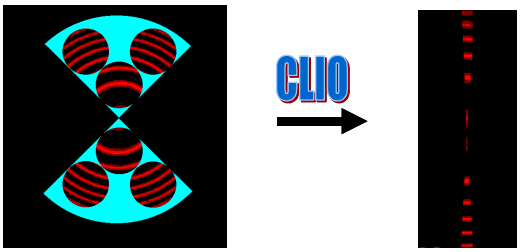

Figure 10: The left figure shows how the Fabry-Perot ring pattern is illuminated with the fiber optic recycler. The relative intensity is not shown to scale. The figure on the right shows the ring pattern after it has been optically transformed by the CLIO optic on the detector.

Telescope

The telescope subsystem consists of one transmitter telescope and one receiver telescope. The telescopes are mounted together on a common gimbal, which rotates 290 degrees in azimuth and is fixed in zenith at a 45-degree elevation. The limitation on azimuth angles is a device that has been designed to protect the fiber optic receiver. This protection device may be disabled to allow 360-degree operation. To meet the performance requirements, the receiver telescope has a usable diameter of 0.5 meters and the transmitter telescope has a clear aperture sufficient to beam expand the laser to the desired beam divergence. The expansion ratio for this beam expander is a function of the field of view of the telescope and the divergence of the laser beam. The main receiving telescope is coupled to the rest of the instrument using fiber optics. We have chosen the gimbaled configuration because it is analogous to that required by a LIDAR system flown on a satellite.

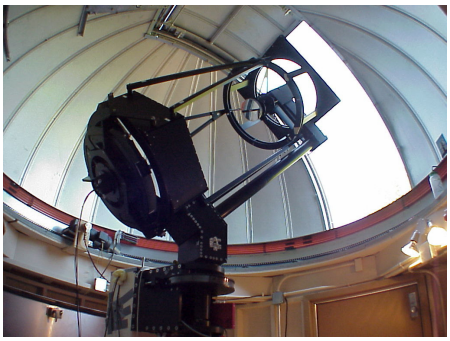

Figure 11: The GroundWinds telescope installed in its dome

Table 5: Viewing [Field of Regard] Parameters.

Telescope diameter	0.5 meters
Effective telescope collecting area	1963 cm^2
Focal Length	2.0 meters
Telescope FOV (half angle)	0.10 mr
Tolerance on Focus and Alignment	0.02mr.
Telescope Transmission	0.81
Solid angle	3.14×10^{-8} sr
Etendue (area * solid angle product)	6.17×10^{-5} cm^2 sr
Zenith Angle	45 degrees
Type of view	Slew & Stare
Integration time at each azimuth	Average 10 second samples on chip

Table 6: Receive Transfer Optics

Fiber Optics	0.4mm diameter
Numerical Aperture	0.22
F/# at exit of fiber	2.3

Laser

The GroundWinds system uses a commercial Nd:YAG laser that meets most of the optical requirements of the space LIDAR, but at considerably lower cost than would be required to procure a copy of a space-qualified engineering model. This laser also has considerably lower maintenance and operational costs associated with it. A custom Continuum 8010 laser was chosen for this system. The selected laser provides ~4 watts of output power at 532 nm. The laser is seeded to obtain a single frequency output, with a bandwidth comparable to that required for a satellite system. The pulse length of this laser was chosen to be somewhat longer than was actually required. The laser's oscillator cavity was modified to provide a 50 ns pulse. Initial assessments indicated that this would provide error margin in spectral resolution at a minimal cost and risk to the project. A pulse length of 8 – 10 ns is typical with this type of laser. In practice, the interferometer is not able to take advantage of the additional resolution that the laser provides with this stretched pulse, and the laser was restored to the standard pulse length of 8 nsec, as its stability is better in that configuration. The laser is fired at a repetition rate of 10 Hz.

Detector

An explanation of the technique used to measure both range and spectral information on the CCD is useful in fully understanding the GroundWinds instrument. During the time following a firing of the laser, the photons received by the telescope and processed through the interferometers, are deposited by the CLIO on a very narrow wedge region in the center of the CCD. This wedge of light is a few pixels wide and extends over the entire length of the device (figure 11). The spectrum of the returning light is displayed along this wedge. In order to separate individual ranges the charge in this narrow wedge on the CCD is electronically translated through the chip during the signal return period. This results in a matrix of charge being deposited in the individual potential wells of the CCD after the return of a single laser light pulse. Figure 12 depicts the CCD rows shifting in order to collect the signal returning from the different altitudes (steps a

through e). At the end of this cycle, the image is shifted back to the start for the next laser pulse (step e to a). Only the segment of the CCD labeled "open" is actually exposed to light.

The resulting linear fringe pattern can be scanned using any one of the many commercially available linear array detectors, such as a CCD. Advantages of a CCD over a conventional IPD are higher quantum efficiency, wider spectral range, lower cost, more flexibility of operation, and simpler electronics.

While the IPD in the HRDI instrument has only 32 rings, a conventional CCD combined with the conical circle-to-line optical system can provide a nearly perfect 500 element ring detector. Furthermore, linear solid-state detectors have advantages in providing high quantum efficiency, small, rugged construction, and low cost. Successful experimental tests of this device have been reported by Hays (1990) and Wang et al. (1994).

The CCD detector is used in a configuration similar to a streak photographic system. The only portion of the chip that is exposed is a few rows of pixels at the chip's

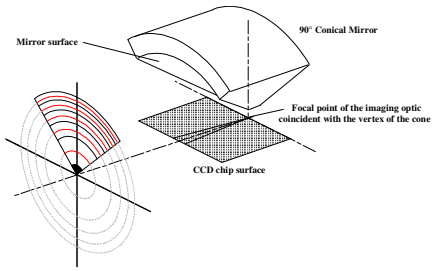

Figure 11: Spatial relationship between the CLIO and the CCD

midpoint. These exposed pixels sit in the image plane of the circle-to-line converter. Just before the laser is fired, the CCD begins shifting the exposed pixels up at a very high rate. This first set of pixels gives dark count and background information. After the laser is fired, the return signal is imaged onto the exposed rows of pixels. While the CCD is shifting the pixels upward, a very small portion of the laser light is leaked into the interferometer and onto the CCD. This provides the laser spectral reference. As the laser pulse is propagating in the atmosphere, the CCD chip is continually shifting data upward so as to save the image data from previous altitudes and expose new pixels. In this way, an image is created, with each row of pixels containing spectral information at a particular altitude. Once the entire return signal is collected, the CCD resets to the bottom and waits for the next return signal from the atmosphere. In this manner, multiple shots may be accumulated on chip, so that the signal to noise may be maximized by not incurring a read noise penalty by reading out more often.

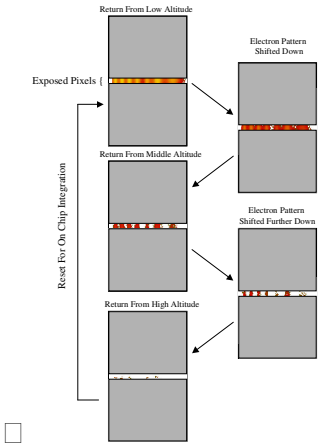

Fig. 12 CCD Lidar Detector time history. As the pulse returns from various altitudes, the image is shifted across the detector (steps a through e). At the end the image is shifted back to the start for the next laser pulse (step e to a). Only the segment of the CCD marked "open" is actually exposed to light.

Table 7: CCD Specifications

CCD Device	SITe CCD
Type	UV Enhanced Back-Thinned CCD Full Frame Transfer (Image/Store)
Format	658 columns x 502 rows image 658 columns x 502 rows storage
Imaging Area	7.8mm x 6.0 mm
Pixel Size	12um x 12um
Full Well Capacity	80Ke- in imaging region (static). 170Ke- in readout register. Specified >30Ke- at 375ns/row shift speed. Measured >38Ke-.
Maximum Dark Count	Mfg. data on process specifies 362 pA/cm^2 @ 293K. Device(s) measure 15.7e-/s/pixel @ 246K.
QE @ 532nm	Mfg. data specifies 80% @ 532 @ 20C. Operation at –50C down to 70%.
CTE	Up to 10 on-chip accumulation cycles with no loss of charge. Specified 0.999995 @ 375ns/row shift.
Detector Cooling	
Type	3 Stage thermoelectric with liquid cooled heat sink.
Cold-Side CCD e	Target is –50C based on dark count data.
Detector Readout	
Shift Register Capacity	160Ke- (TBR)
Non-Linearity	Not specified.
Readout Noise	Measured at 22e- to 26e- RMS in low gain, low bandwidth mode. Conversion gain is 0.6 e-/DN at low gain and 3.1e-/DN at high
Row Shift Direction	Bi-directional (up or down) by command
Row Shift Rate	375ns/row maximum. Limited by ability to charge/discharge clock lines and meet ESD limitations.
On-Chip Integration	Design accommodates 100 on-chip accumulation cycles and intermediate readout before full frame readout.
Vertical Retrace Time	0.2 millisecond possible. Other restrictions apply.
Readout Rate	Best performance at 50K pixels/second. Can run at 500K d.
A/D Resolution	14bits. MSB justified.

3. DATA

The data products generated by the GroundWinds instrument are provided in various processing levels.

Table 8: Data Processing Formats

Level	Description	Resolution
0	Raw spectra vs. time from CCD	1 / 10 second
1	Inverted atmospheric parameters	10 sec / 250 meters
2	Inverted atmospheric parameters	50 sec / 250 meters
3	Net CDF atmospheric parameters	1 min / 250 meters: .5 – 3 km alt 1 min / 1000 meters: 3 – 15 km alt

The level 2 data is being presented in this paper due to its higher resolution. However, level 3 data is better suited to applications seeking to utilize wind data because level 2 altitude resolution is usually unnecessary. The data from the LIDARFest 2000 campaign was the first significant quantity of data that had been acquired with the GroundWinds instrument. The quality and quantity of the data improved over the course of the 2 week campaign, as several operational issues were still being worked out at its beginning. Data from the last day was acquired without knowledge of the measurements of the other instruments or radiosondes. This data was of the highest quality and taken during the most favorable atmospheric conditions. This data is shown in figures 13 and 14. This data set is interesting for a number of reasons. First, it is the longest continuous data collection taken during the campaign, and all instruments were fully operational. In these figures, the horizontal component of wind is shown in a fixed azimuth direction. This observation window also allowed an opportunity to capture instrument performance as a cloud drifted into the field of view at approximately 5 km. Data before and after this event were recorded. At approximately 1360 min, the blocking filter was removed from the system, allowing the instrument to operate with increased sensitivity without solar background. The effect of this is seen after the cloud moves out of the field of view.

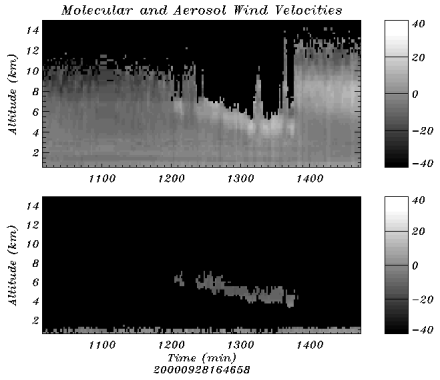

Figure 13: Wind velocities measured from the molecular and aerosol channels. These are a 1 minute integration time with a vertical resolution of .25 km below 3 km, and 1 km above 3km.

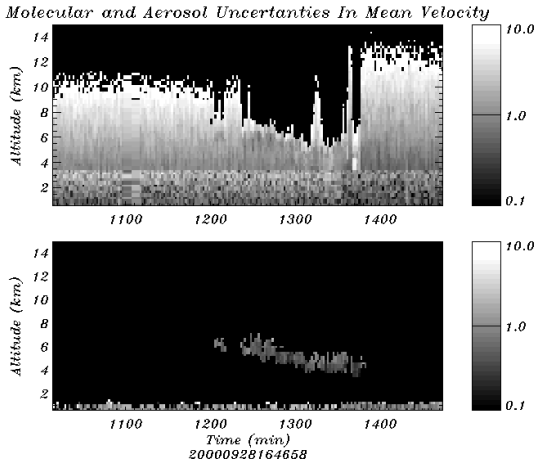

Figure 14: These uncertainties are standard deviations of the data points that were averaged in order to fit the data onto the grid that all instruments used (the same as in figure 12).

Figure 15 shows several comparisons between the GroundWinds instrument and the radiosondes for data sets on the 25th and 27th of September. These show very good agreement, but it is not clear that the agreement at higher altitudes is statistically significant, since the radiosondes was 50 – 100 km downrange at the higher altitudes.

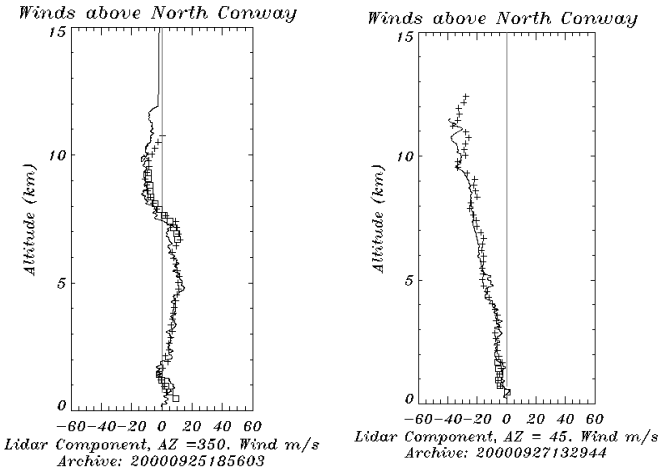

Figure 15: Two plots showing altitude profiles in the azimuth direction that GroundWinds was looking. The aerosol channel is shown via a square, and the molecular channel is shown with an asterisk. The radiosondes is the solid line. Note that on the 25th aerosol measurements were made from a thin cloud between 6 and 9 km.

4. CONCLUSIONS

The data presented herein allows us to conclude that the direct detection method of Doppler LIDAR can be used to measure winds in the troposphere. The detection efficiency of this system could be improved in several respects by the use of higher quality and/or custom designed components that were not available largely because of cost considerations. Examples include the read noise characteristics of the CCD detector, the quality of the CLIO optic, and the quantum efficiency of the CCD detector at cold temperatures. It is expected that the GroundWinds Hawaii instrument will build upon the success of this instrument, but be superior in several respects. In particular, the read noise characteristics of the detector will be much improved.

The authors realize the importance of fully understanding this system's photometric efficiency and error budgets in the extrapolation of this work to future systems. At present, these parameters are being quantified and will be reported in a future paper. Additionally, the optimal recycling configuration, and the benefits of the recycling technique must be quantified. These are the subjects of ongoing work with this and the Hawaii system.

ACKNOWLEDGEMENTS

The authors and the staff of Michigan Aerospace Corporation would like to thank NOAA for their support, as well as the staff of the University of New Hampshire and the Mount Washington Observatory. This success of this project would not have been possible without the vision of Dr. Berrien Moore. The efforts of Dr. James Ryan, Lynn Rosentrater, Steven Turco, Michelle Day, and Ken Rancourt were particularly critical to the successful outcome of the validation campaign. Additionally, the investment made in this project by our suppliers made a difference between success and failure. We would like to thank Continuum, Torus Technologies, PixelVision and Process Results for their contributions to the development of this technology.

REFERENCES

Hays, Paul. 1990. Circle to line interferometer optical system. *Applied Optics, us.* 29(1 April): 1482-1489.

Hays, Paul, et al 1993. The High-Resolution Doppler Imager on the Upper Atmosphere Research Satellite. *Journal of Geophysical Research* Vol.98 No. D6:10,713-10,723.

Jacquinot, P. 1954. The Luminosity of Spectrometers with Prisms, Gratings or Fabry-Perot Etalons. *American Journal Optical Society.* 44:761-765.

Killeen, Timothy L. and Hays, P.B. 1984. Doppler line profile analysis for a multichannel Fabry-Perot interferometer. *Applied Optics, us.* 23(15 February): 612-620.

Rees, David and McDermid, I Stuart. 1990. Doppler lidar atmospheric wind sensor: Reevaluation of a 355-nm incoherent Doppler lidar. *Applied Optics, us.* 29(1 October):4133-4144.

Wang, C. C. et al. 1994. University of Michigan Ground-Based Circle-to-Line Fabry-Perot Interferometer and its Applications in Mesosphere and Lower Thermosphere Dynamics Studies. *Optical and Spectroscopic Techniques and Instrumentation for Atmospheric and Space Research, San Diego, SPIE Proceedings,* 2266:133-142.